Liquid Phase Diffusion of Branched Alkanes in Silicalite

Kader Lettat
Institut Français du Pétrole, Catalysis and Separation Division, BP 3, 69390 Vernaison, France

Laboratoire des Sciences du Génie Chimique, CNRS-ENSIC-INPL, 1, rue Grandville, BP 451, F-54001 Nancy cedex, France

Elsa Jolimaitre
Institut Français du Pétrole, Catalysis and Separation Division, BP 3, 69390 Vernaison, France

Mélaz Tayakout
IRCELYON, 2 Avenue Einstein, 69626 Villeurbanne, Cedex, France

Daniel Tondeur
Laboratoire des Sciences du Génie Chimique, CNRS-ENSIC-INPL, 1, rue Grandville, BP 451, F-54001 Nancy cedex, France

DOI 10.1002/aic.12268
Published online April 28, 2010 in Wiley Online Library (wileyonlinelibrary.com).

*This work provides a new mass transfer model based on the Maxwell–Stefan theory, especially adapted to represent adsorbed phase multicomponent diffusion at high-adsorbent loading. In our model—contrarily to the well-known model developed by Krishna et al. (*Chem Eng Sci. *1990;45:7:1779–1791;* Gas Sep Purif. *1993;7:91–104;* J Phys Chem B. *2005;109:6386–6396)—the hypothesis that the micropores are saturated does not imply a dependency between the adsorbed phase diffusion coefficients. Experimental liquid phase breakthrough curves of 2-methylpentane (2MP), 3-methylpentane (3MP), 2,3-dimethylbutane (23DMB), and 2,2-dimethylbutane (22DMB) were measured at 458 K in silicalite. The self-diffusion coefficients and Langmuir parameters of the different species were determined using binary exchange breakthrough curves. The Maxwell–Stefan diffusion coefficients obtained for the different isomers are in the order* $D_{3MP,nc+1} > D_{2MP,nc+1} \gg D_{23DMB,nc+1}$, *and vary between* 4×10^{-15} m^2 s^{-1} *for 3MP to* 6×10^{-16} m^2 s^{-1} *for 23DMB. The 22DMB diffusion coefficient is so low that it could not be estimated (the quantity of 22DMB entering silicalite during the experiment is not significant). The model was then validated by comparing experimental breakthrough curves at different feed concentrations and simulations using the independently estimated parameters. Even though the diffusion coefficients of the different isomers vary by one order of magnitude, the agreement between simulated and experimental curves is very satisfactory, showing the good predictive power of our model.*
 AIChE J, 57: 319–332, 2011
Keywords: adsorption, liquid phase, diffusion, mixtures, zeolites, modeling

Introduction

In the literature, diffusion of mixtures in microporous solids is usually studied in the low-concentration regime, where the solid porosity is not fully occupied by adsorbed

Correspondence concerning this article should be addressed to E. Jolimaitre at elsa.jolimaitre@ifp.fr.

molecules. This corresponds to experimental conditions that are unfavorable to high-capacity adsorption, typically gas phase at low-partial pressures and/or high temperatures.[1] In such conditions, exploitation of the experimental data can be carried out by models such as those developed by Taylor and Krishna[2] (theory of Maxwell–Stefan applied to the diffusion in solids via the model known as the "dusty gas model").

When separation by adsorption is carried out in the liquid phase, which is industrially very frequent and appropriate for the mixture of C6 considered here, the confinement of the molecules in the porous network is very high. Consequently, additional constraints appear in the solid. The first type of constraints is volumetric or steric, and they can be described differently depending on the size of the porosity.

- In the macro/mesoporosity, where the size of the molecules is much smaller than the pores, a "classical" volume constraint can be added to the mass balances: a molecule can penetrate the porosity only if the corresponding volume is available within the network. A convective flow is then introduced to take these phenomena into account.
- In the microporosity, where the size of the molecules is very close to that of the pores, the constraints can be introduced via the adsorption equilibrium and by fixing an adsorbed phase molecular volume for each molecule. In our case, the chosen adsorption equilibrium is the generalized monosite Langmuir isotherm and the adsorbed phase molar volume is supposed to be that of the liquid phase at the same temperature. In our experimental conditions, the Langmuir parameters are so high, that the quantities adsorbed always tend toward saturation.

Furthermore, as will be shown in this article, the classical adsorbed phase diffusion models based on the Maxwell–Stefan equation cannot represent correctly multicomponent diffusion close to saturation.

A new model was therefore developed and validated by comparison with experimental liquid phase breakthrough curves for ternary mixtures of various hexane isomers in silicalite. The model represents the adsorbed phase diffusion of these molecules with a high degree of accuracy, even though the diffusion kinetics of these molecules in silicalite is very different.

Model

Model hypothesis

The fixed-bed column is assumed to be packed with bidisperse pellets composed of adsorbent crystals held together by a binder. Such a system is classically divided into three phases: the bulk fluid (extragranular fluid phase), the fluid-filled macroporosity of the pellets, and the crystals containing the microporosity where adsorption occurs.[3] The premises and hypotheses concerning these different levels of porosity are listed below.

1. The pellets and the microporous crystals are supposed to be spherical.

2. The flow in the packed bed is represented by a cascade of continuous stirred tank reactors (CSTRs) in series. In our experimental conditions, axial dispersion in the extragranular fluid phase is small ($Pe > 100$), and the breakthrough curves can be very steep. Calculating the axial dispersion with well-known correlations yields a very high number of CSTRs (450). However, only 150 reactors were used in the simulations, as a compromise between a good curve fitting and a reasonable calculation time, while adding negligible dispersion with respect to the contribution of internal resistances.

3. Dead volumes before and after the adsorption column where accounted for and also represented by a cascade of CSTRs.

4. Mass transfer resistances at the pellet surface and in the macropores are lumped into a single external film mass transfer coefficient k^m. A stagnant film around the zeolite crystals is also introduced, with a corresponding mass transfer coefficient k^c. However, the value of this mass transfer coefficient is always chosen large so that the corresponding transfer resistance is negligible, and is only useful to simplify the numerical resolution of the equations.

5. The liquid mixture is ideal (in the extragranular fluid phase and in the macropores).

6. The variation of the fluid velocity (due to adsorption and to the different molar volumes of the molecules) is taken into account. Molar volumes were obtained from the thermodynamic properties library DIPPR.

7. Convection inside the macropores is taken into account. When the volumetric flow leaving (or entering) the adsorbent is not constant, volume constrains induce a convective flow in the macropores.

8. The column is isothermal. This assumption is supported by two particular properties of this system. The adsorbent is always close to saturation, so the total number of molecules present in the adsorbed phase does not vary much (one molecule is more or less replaced by another molecule). Moreover, the heats of adsorption of all the species are practically equivalent.

9. The adsorption equilibrium is represented by the generalized Langmuir model. The local equilibrium hypothesis is assumed along the whole radius of the crystal.

10. Mass transfer in the crystallites is described by the Maxwell–Stefan equations adapted to diffusion in a porous solid (dusty gas model).

The transport model proposed in this article is thus comparable with the well-known model published by Krishna.[1] However several modifications are introduced, the reasons and consequences of which will be clarified in this article:

- Volume constraints are introduced in the microporosity (zeolite pores). The adsorbed phase molar volumes are supposed to be the same as in the fluid phase for all molecules. Consequently, the solid is not represented by vacant sites but by the residual adsorbent volume (the volume which is not occupied by the adsorbed molecules). Moreover, the force exerted on species i due to the friction with the solid is taken as proportional to the volume fraction (instead of the molar fraction) of solid.
- The reference for the diffusion fluxes in the microporosity is the barycentre of the volume of all species, including the solid matrix. Consequently, the flux corresponding to the solid is not set to zero, but instead is taken as a variable.
- The state variable for the adsorbed phase is the fictitious fluid in equilibrium with the adsorbed phase. It has been shown in previous work[4] that this variable change produces a more compact equation system.

11. The size of the diffusing molecules being very close to the pore radius, it is assumed that there is no possibility of counterdiffusion between the adsorbed species i and j inside single pores (diffusion with no mutual interaction).

The preceding hypotheses lead to the set of equations presented in the next sections. The material balances that are classical and can be found in earlier publications (e.g., Refs. 1,3,5,9,10) and are not developed in detail. On the other hand, the equations relative to the microscopic level are specific of the present model, and are given some more attention here.

Material balances

In the following, ϕ designates the volume fractions, with subscripts corresponding to the species, the first superscript to the phase (f, m, or c for fluid, macropore, or crystal, respectively), and the second superscript to the index of the CSTR; nc designates the number of components.

In the Bulk Fluid. For the kth CSTR

$$\begin{bmatrix} \frac{L.\varepsilon_i}{u_{\mathrm{f}}^0}.\frac{\partial \phi_1^{\mathrm{f},k}}{\partial t} \\ . \\ . \\ . \\ \frac{L.\varepsilon_i}{u_{\mathrm{f}}^0}.\frac{\partial \phi_{\mathrm{nc}-1}^{\mathrm{f},k}}{\partial t} \end{bmatrix} = \begin{bmatrix} \alpha^{k-1}.\phi_1^{\mathrm{f},k-1} - \alpha^k.\phi_1^{\mathrm{f},k} - \frac{L.\varepsilon_i}{u_{\mathrm{f}}^0}.\frac{3}{R_p}.\frac{(1-\varepsilon_i)}{\varepsilon_i}.v_1.N_1^{\mathrm{mac},k} \\ . \\ . \\ . \\ \alpha^{k-1}.\phi_{\mathrm{nc}-1}^{\mathrm{f},k-1} - \alpha^k.\phi_{\mathrm{nc}-1}^{\mathrm{f},k} - \frac{L.\varepsilon_i}{u_{\mathrm{f}}^0}.\frac{3}{R_p}.\frac{(1-\varepsilon_i)}{\varepsilon_i}.v_{\mathrm{nc}-1}.N_{\mathrm{nc}-1}^{\mathrm{mac},k} \end{bmatrix} \quad (1)$$

with:

$$\alpha^k = \frac{u_{\mathrm{f}}^k}{u_{\mathrm{f}}^0} = 1 - \frac{L.\varepsilon_i}{u_{\mathrm{f}}^0}.\frac{1-\varepsilon_i}{\varepsilon_i}.\frac{3}{R_p}.\sum_{l=1}^{k}\sum_{j=1}^{\mathrm{nc}} v_j.N_j^{\mathrm{mac},l} \quad (2)$$

These equations result from a simple mass balance on the kth CSTR.

The volume constraints associated to these equations are:

$$\sum_{j=1}^{\mathrm{nc}} \phi_j^{\mathrm{f},k} = 1 \quad (3)$$

In the Macroporosity. For the kth CSTR, the material balance in the macroporosity gives:

$$\begin{bmatrix} \frac{\partial \phi_1^{\mathrm{m},k}}{\partial t} \\ . \\ . \\ . \\ \frac{\partial \phi_{\mathrm{nc}-1}^{\mathrm{m},k}}{\partial t} \end{bmatrix} = \begin{bmatrix} \frac{3}{R_p.\varepsilon_p}.v_1.N_1^{\mathrm{mac},k} - \frac{3}{R_{\mathrm{c}}}.\frac{1-\varepsilon_p}{\varepsilon_p}.v_1.N_1^{\mathrm{mic},k} \\ . \\ . \\ . \\ \frac{3}{R_p.\varepsilon_p}.v_{\mathrm{nc}-1}.N_{\mathrm{nc}-1}^{\mathrm{mac},k} - \frac{3}{R_{\mathrm{c}}}.\frac{1-\varepsilon_p}{\varepsilon_p}.v_{\mathrm{nc}-1}.N_{\mathrm{nc}-1}^{\mathrm{mic},k} \end{bmatrix} \quad (4)$$

The volume constraints associated to these equations are:

$$\sum_{j=1}^{\mathrm{nc}} \phi_j^{\mathrm{m},k} = 1 \quad (5)$$

The flux between the fluid phase and the macropores for component j is:

$$N_j^{\mathrm{mac},k} = \frac{N_T^{\mathrm{mac},k}}{C_T^{\mathrm{m},k}.v_j}.\left[\frac{\phi_j^{\mathrm{f},k} - \phi_j^{\mathrm{m},k}.\exp\left(-\frac{N_T^{\mathrm{mac},k}}{k_j^{\mathrm{m}}.C_T^{\mathrm{m},k}}\right)}{1-\exp\left(-\frac{N_T^{\mathrm{mac},k}}{k_j^{\mathrm{m}}.C_T^{\mathrm{m},k}}\right)}\right] \quad (6)$$

with

$$\frac{1}{k_j^{\mathrm{m}}} = \frac{1}{k_j^{\mathrm{f}}} + \frac{R_p}{5.\varepsilon_p.D_j^{\mathrm{mac}}} \quad (7)$$

$$C_T^{\mathrm{m},k} = \frac{1}{v_{\mathrm{nc}}} + \sum_{j=1}^{\mathrm{nc}-1}\left[\frac{\phi_j^{\mathrm{m},k}}{v_j}.\left(1-\frac{v_j}{v_{\mathrm{nc}}}\right)\right] \quad (8)$$

The total convective flux in the macropores can be calculated from the global material balance on the macropores:

$$\frac{3}{R_p.\varepsilon_p}.N_T^{\mathrm{mac},k} = \sum_{j=1}^{\mathrm{nc}}\frac{1}{v_j}.\frac{\partial \phi_j^{\mathrm{m},k}}{\partial t} + \frac{3}{R_{\mathrm{c}}}.\frac{1-\varepsilon_p}{\varepsilon_p}.N_T^{\mathrm{mic},k} \quad (9)$$

The material balance inside the pellets is more complex than what can usually be found in the literature, because a convective flow was introduced, to take into account the volume constraints in the macroporosity. For more precisions on the derivation of these equations, see the article by Leinekugel-le-Cocq et al.,[5] who first derived these equations.

In the Crystal. In the kth CSTR, the equations associated to the material balance of the jth component plus one associated to the solid in the crystal (corresponding to the subscript nc + 1) can be written as:

$$\frac{\partial \phi_j^{\mathrm{c},k}}{v_j.\partial t} = -\frac{1}{r_{\mathrm{c}}^2}.\frac{\partial\left(r_{\mathrm{c}}^2.N_j^{\mathrm{c},k}\right)}{\partial r_{\mathrm{c}}} \quad j = 1, \mathrm{nc}+1 \quad (10)$$

The constraints associated to these equations are:

1. One constraint corresponding to the volume balance in the microporosity, including the solid:

$$\sum_{j=1}^{\mathrm{nc}+1} \phi_j^{\mathrm{c},k} = 1 \quad (11)$$

The volume fractions ϕ^{c} are defined with respect to the total volume of the crystal, so that $\phi_{\mathrm{nc}+1}^{\mathrm{c}}$ represents a volume fraction unoccupied by the adsorbable molecules.

2. One constraint corresponding to the global volumetric flux balance

$$\sum_{j=1}^{\mathrm{nc}+1} v_j \cdot N_j^{\mathrm{c},k} = 0 \quad (12)$$

This equation deserves some comments. Noting that the product $v_j N_j$ for the adsorbing species is a volume flux (dimension of a velocity), the term corresponding to nc + 1 thus globally represents a volume flux of the solid matrix. We do not have to define a molar volume nor a molar flux of the solid, only their product has a meaning, but we chose to retain the general form of Eq. 12.

The summation over nc + 1 species of these volume fluxes is zero only in an appropriate reference frame, where the average velocity also accounts for the volume fraction of all the nc + 1 species. This reference frame applies coherently to all fluxes used in this text and entails no practical complication.

The state variable chosen in the present model is a nondimensional concentration in the fictitious fluid phase in equilibrium with the adsorbed phase and is defined by:

$$\phi_j^{*,k} = C_j^{*,k} \cdot v_j. \tag{13}$$

The relation between the two variables $\phi_j^{*,k}$ and $\phi_j^{c,k} = q_j^{c,k} v_j$ is given by the generalized Langmuir law as follows:

$$\phi_j^{c,k} = \frac{q_j^{sat}.b_j.\phi_j^{*,k}}{1+\sum_{l=1}^{nc}\frac{b_l\phi_l^{*,k}}{v_l}} \quad j = 1, \ldots, nc \tag{14}$$

As mentioned above, $\sum_{j=1}^{nc} \phi_j^{c,k}$ is the total volume fraction occupied by the adsorbed phase in the crystal, and $\phi_{nc+1}^{c,k}$ is the unoccupied volume fraction. To clarify this, consider a situation close to saturation and for which all the molecules have the same molar volume and the same concentration at saturation ($q_j^{sat} = q^{sat}$; $v_j = v\ \forall j$). Then, as saturation is approached:

The sum $\sum_{j=1}^{nc} \phi_j^{c,k}$ tends toward $q^{sat} \cdot v$, which can be seen as the maximum volume fraction available for the studied molecules at the given experimental conditions,

$\phi_{nc+1}^{c,k}$ tends toward $1 - q^{sat} \cdot v$, which is the solid volume fraction in the crystal.

On the contrary, the variables $\phi_j^{*,k}$ are unconstrained. Introducing this variable $q_j^{*,k}$ and the constraints corresponding to Eqs. 11 and 12 into Eq. 10 gives:

$$\begin{bmatrix} q_1^{sat}b_1\left(1+\sum_{i=2}^{nc}\frac{b_i.\phi_i^{*,k}}{v_i}\right) & \ldots & -q_1^{sat}b_1b_{nc}\frac{\phi_1^{*,k}}{v_1}. \\ . & & . \\ . & & . \\ . & & . \\ -q_{nc}^{sat}b_{nc}b_1\frac{\phi_{nc}^{*,k}}{v_{nc}} & \ldots & q_{nc}^{sat}b_{nc}\left(1+\sum_{i=1}^{nc-1}\frac{b_i\phi_i^{*,k}}{v_i}\right) \end{bmatrix} \begin{bmatrix} \frac{\partial\phi_1^{*,k}}{v_1.\partial t} \\ . \\ . \\ . \\ \frac{\partial\phi_{nc}^{*,k}}{v_{nc}.\partial t} \end{bmatrix}$$

$$= \left(1+\sum_{i=1}^{nc}\frac{b_i.\phi_i^{*,k}}{v_i}\right)^2 \begin{bmatrix} -\frac{1}{r_c^2}\frac{\partial\left(r_c^2N_1^{c,k}\right)}{\partial r_c} \\ . \\ . \\ . \\ -\frac{1}{r_c^2}\frac{\partial\left(r_c^2N_{nc}^{c,k}\right)}{\partial r_c} \end{bmatrix} \tag{15}$$

The boundary conditions in the kth CSTR are:

$$\forall t \quad \text{at } r_c = 0 \quad N_j^{c,k} = 0 \quad j = 1, \text{nc} \tag{16}$$

$$\forall t \quad \text{at } r_c = R_c \quad N_j^{c,k} = \frac{k_j^c}{v_j}.\left(\phi_j^{m,k} - \phi_j^{*,k}\right) \quad j = 1, \text{nc} \tag{17}$$

Expression of the diffusion fluxes in the micropores

To complete this model, an expression for the diffusion fluxes in the micropores $N_j^{c,i}$ has to be established. Our model is based on the dusty gas model, coupled with the Maxwell–Stefan equations[6,10]. As mentioned before, the flux of the solid is taken into account in this model and the friction between species j and the solid is proportional to the volume fraction of solid. The size of the diffusing molecules being very close to the pore radius, it is assumed that there is no possibility of counterdiffusion between the adsorbed species i and j (diffusion with no mutual interaction), and therefore the drag coefficients representing molecule–molecule interactions are not taken into account ($\frac{RT}{D_{ij}} = 0$, and the binary crossdiffusion coefficients tend to infinity). With all these considerations, the Maxwell–Stefan equation gives:

$$\frac{\phi_j^{c,k}}{v_j \cdot RT}\nabla_{T.P}\mu_j^{c,k} = -\frac{1}{D_{j,NC+1}}.\left(\phi_{nc+1}^{c,k}.N_j^{c,k} - \frac{\phi_j^{c,k}}{v_j}.v_{nc+1}N_{nc+1}^{c,k}\right) \quad j = 1, \ldots, nc \tag{18}$$

Notice that the only diffusion coefficients appearing in this equation, $D_{j,nc+1}$ are the single component diffusion coefficients of the species in the solid matrix.

The new state variable corresponding to the fictitious fluid phase is introduced into the Maxwell–Stefan equations via the generalized Langmuir law (Eq. 14). The local equilibrium hypothesis implies the equality of chemical potentials between the adsorbed phase and the fictitious fluid phase along the whole radius of the crystal. If this fictitious phase is considered as an ideal fluid then the chemical potential can be written as follows:

$$\mu_j^{*,k} = \mu_j^{c,k} = \mu_j^{*,ref} + RT\ln\frac{C_j^{*,k}}{C_T^{*,k}} \tag{19}$$

Supposing the total concentration of the hypothetical fluid $C_T^{*,k}$ constant:

$$\nabla\mu_j^{c,k} = RT.\nabla\ln C_j^{*,k} = RT.\frac{\nabla\phi_j^{*,k}}{\phi_j^{*,k}} \tag{20}$$

Introducing the Langmuir law into Eq. 20 gives:

$$\frac{\phi_j^{c,k}}{RT}\nabla_{T,P}\mu_j^{c,k} = \frac{q_j^{sat}b_j}{1+\sum_{i=1}^{nc}\frac{b_i\phi_i^{*,k}}{v_i}} \cdot \nabla\phi_j^{*,k} \tag{21}$$

Two additional constraints have to be taken into account.

For molecules with different molar volumes, the global flux balance, Eq. 12, is rewritten:

$$v_{\mathrm{nc}+1} \cdot N_{\mathrm{nc}+1}^{\mathrm{c},k} = -\sum_{i=1}^{\mathrm{nc}} v_i N_i^{\mathrm{c},k} \tag{22}$$

The volume constraint in the crystals, Eq. 11, gives:

$$\phi_{\mathrm{nc}+1}^{\mathrm{c},k} = 1 - \sum_{i=1}^{\mathrm{nc}} \phi_i^{\mathrm{c},k} \tag{23}$$

Introducing Eqs. 21–23 into the Maxwell–Stefan Eq. 18 yields the following system of equations for the kth CSTR, relating the concentration gradients to the fluxes:

$$\begin{bmatrix} \frac{q_1^{\mathrm{sat}}.b_1}{v_1}\frac{\partial \phi_1^{*,k}}{\partial r_{\mathrm{c}}} \\ \cdot \\ \cdot \\ \cdot \\ \cdot \\ \frac{q_{\mathrm{nc}}^{\mathrm{sat}}.b_{\mathrm{nc}}}{v_{\mathrm{nc}}}\frac{\partial \phi_{\mathrm{nc}}^{*,k}}{\partial r_{\mathrm{c}}} \end{bmatrix} = - \begin{bmatrix} \frac{1}{D_{1,\mathrm{nc}+1}}\left(1 + \sum_{i=1}^{\mathrm{nc}} \frac{b_i \phi_i^{*,k}}{v_i} - \sum_{i=2}^{\mathrm{nc}} q_i^{\mathrm{sat}} b_i \phi_i^{*,k}\right) & \ldots & \left(\frac{q_1^{\mathrm{sat}} b_1 \phi_1^{*,k}}{D_{1,\mathrm{nc}+1}}\right) \\ & & \cdot \\ & & \cdot \\ & & \cdot \\ \left(\frac{q_{\mathrm{nc}}^{\mathrm{sat}} b_{\mathrm{nc}} \phi_{\mathrm{nc}}^{*,k}}{D_{\mathrm{nc},\mathrm{nc}+1}}\right) & \ldots & \frac{1}{D_{\mathrm{nc},\mathrm{nc}+1}}\left(1 + \sum_{i=1}^{\mathrm{nc}} \frac{b_i \phi_i^{*,k}}{v_i} - \sum_{i=1}^{\mathrm{nc}-1} q_i^{\mathrm{sat}} b_i \phi_i^{*,k}\right) \end{bmatrix} \begin{bmatrix} N_1^{\mathrm{c},k} \\ \cdot \\ \\ \\ \\ \vdots \\ N_{\mathrm{nc}}^{\mathrm{c},k} \end{bmatrix} \tag{24}$$

The flux vector N can then be obtained from Eq. 24 by inversion of the matrix, which is nonsingular, square, and of rank nc. The fluxes are then substituted into Eq. 15.

Global Material Balance. The global material balance for each component is calculated and verified for all simulations. The corresponding equation is:

$$\frac{\phi_j^{\mathrm{f},0}}{v_j} u_{\mathrm{f}}^0 \cdot t = \int_0^t \frac{\phi_j^{f,\mathrm{NZ}}}{v_j} u_{\mathrm{f}} \cdot dt + \frac{L}{v_j} \sum_{k=1}^{\mathrm{NZ}} \left(\phi_j^{\mathrm{f},k} \varepsilon_i + \phi_j^{\mathrm{m},k}(1-\varepsilon_i)\varepsilon_p + \bar{\phi}_j^{\mathrm{c},k}(1-\varepsilon_i)\left(1-\varepsilon_p\right)\right) \tag{25}$$

where NZ is the total number of CSTRs.

Discussion on the application of the dusty gas model to the Maxwell–Stefan equations

Krishna[2] was the first to propose a description of diffusion in the adsorbed phase based on the generalized Maxwell–Stefan equations coupled with the dusty gas model [the solid is treated as the $(n + 1)$th component]. Moreover, Krishna and coworkers[8,9] have thoroughly studied the validity of this type of model for diffusion of hexane isomers in silicalite, i.e., precisely the system considered in this article. The aim of this discussion is therefore to explain for what purpose a different model was developed for this study.

In this article, friction between the different molecules in the adsorbed phase is always neglected, and only the interactions between the species and the solid matrix are accounted for (diffusion with no mutual interaction). As a result, only nc "diagonal" diffusion coefficients are introduced. This by no means implies that there is no crosscoupling between the species in the diffusion process, but these couplings are due to the volume constraints and to the Gibbs–Duhem constraint discussed below. An important issue is then the independence of the diagonal coefficients, to which we now give some attention. The conclusions developed here are therefore only valid in that particular theoretical framework.

Introduction of the Gibbs–Duhem Constraint in the Maxwell–Stefan Equation. Conceptually, the Maxwell–Stefan equation derives from the energy balance exerted on a molecule during its motion in the solid[1]:

$$\frac{\nabla \mu_j}{R \cdot T} = -\sum_{\substack{i=1 \\ i \neq j}}^{\mathrm{nc}+1} \frac{x_i}{D_{ji}} \cdot \left(u_j - u_i\right) \quad j = 1, \mathrm{nc} \tag{26}$$

For diffusion with no mutual interaction, only the solid, i.e., the (nc + 1)th species, exerts a friction on species j, therefore:

$$\frac{\nabla \mu_j}{R \cdot T} = -\frac{x_{\mathrm{nc}+1}}{D_{j,\mathrm{nc}+1}} \cdot \left(u_j - u_{\mathrm{nc}+1}\right) \tag{27}$$

Table 1 shows how the Fickian form of the diffusion matrix can be derived from Eq. 27, depending on the different assumptions (Krishna's or this work's). Notice that the Maxwell–Stefan diffusion coefficients are not defined exactly in the same way: $Đ_{j,\mathrm{nc}+1} = \frac{D_{j,\mathrm{nc}+1}}{\theta_{\mathrm{nc}+1}}$ where $Đ_{j,\mathrm{nc}+1}$ is Krishna's diffusivity whereas $D_{j,\mathrm{nc}+1}$ is this work's.

In both cases, the Gibbs–Duhem equation has to be respected:

$$\sum_{j=1}^{\mathrm{nc}+1} q_j \nabla \mu_j^{\mathrm{c}} = 0 \tag{28}$$

If Eq. 28 is applied to Krishna's Maxwell–Stefan diffusion equation, and supposing that the $(n + 1)$th species flux is cancelled, we get:

$$\sum_{j=1}^{\mathrm{nc}} \frac{N_j}{Đ_{j,\mathrm{nc}+1}} = 0 \tag{29}$$

Table 1. Derivation of Maxwell–Stefan's Equation Depending on the Hypothesis

	$x_j \cdot \frac{\nabla \mu_j}{R \cdot T} = -\frac{x_{nc+1}}{D_{j,nc+1}} \cdot (u_j - u_{nc+1})$	
	Krishna[1,10,11]	This work
Representation of (nc + 1)th species	The adsorbent is characterized by a given concentration of sites per unit of surface (or volume). $\theta_j = \frac{q_j}{q_j^{sat}}$ with: q_j^{sat}: total number of sites for species j per unit surface (or volume) q_j: number of sites occupied by species j per unit surface (or volume) The (nc + 1)th species is the vacant sites. $\theta_{nc+1} = 1 - \sum_{j=1}^{nc} \theta_j$ with: θ_{nc+1}: fractional loading of vacant sites	The adsorbent is characterized by the total (and fixed) volume of the crystal. $\phi_j^c = q_j \cdot v_j$ where v_j is the molar volume of species j in the adsorbed phase and q is a molar concentration (not a concentration of sites) ϕ_j^c ($j \neq$ nc + 1): volume occupied by species j per unit volume of crystal The (nc + 1)th species is the crystal volume not occupied by adsorbed molecules. $\phi_{nc+1}^c = 1 - \sum_{j=1}^{nc} \phi_j^c$ with: ϕ_{nc+1}^c: volume of the (nc + 1)th species per unit volume of crystal
Expression of the fluxes	$N_j = q_j \cdot u_j \; j = 1$, nc The solid flux is neglected: $N_{nc+1} = 0$	$N_j = \frac{\phi_j^c}{v_j} \cdot u_j \quad j = 1, nc+1$ The non-zero solid flux is taken into account in the general reference frame of the dusty gas model: $v_{nc+1} \cdot N_{nc+1} = -\sum_{j=1}^{nc} v_j N_j$
Expression for x_{nc+1}	x_{nc+1} is the mole fraction of vacant sites $x_{nc+1} = \theta_{nc+1}$	x_{nc+1} is the volume fraction unoccupied by the adsorbed molecules $x_{nc+1} = \phi_{nc+1}^c$
Resulting Maxwell–Stefan diffusion equation (for single-file diffusion)	$\theta_j \cdot \frac{\nabla \mu_j}{RT} = -\frac{\theta_{nc+1}}{D_{j,nc+1} \cdot q_j^{sat}} \cdot N_j$ The Maxwell–Stefan diffusion coefficient $Đ_j$ is defined by $Đ_{j,nc+1} = \frac{D_{j,nc+1}}{\theta_{nc+1}}$ giving: $\theta_j \cdot \frac{\nabla \mu_j}{RT} = -\frac{1}{Đ_{j,nc+1} \cdot q_j^{sat}} \cdot N_j$	$\frac{\phi_j^c}{v_j} \cdot \frac{\nabla \mu_j}{RT} = -\frac{v_{nc+1}}{D_{j,nc+1}} \left(\frac{\phi_{nc+1}^c}{v_{nc+1}} \cdot N_j - \frac{\phi_j^c}{v_j} \cdot N_{nc+1} \right)$ Taking into account the previous equations $\phi_{nc+1}^c = 1 - \sum_{j=1}^{nc} \phi_j^c$ and $v_{nc+1} \cdot N_{Nc+1} = -\sum_{j=1}^{nc} v_j N_j$ the MS equation becomes: $\frac{\phi_j^c}{v_j} \cdot \frac{\nabla \mu_j}{RT} = -\frac{1}{D_{j,nc+1}} \left(\left(1 - \sum_{k=1}^{nc} \phi_k^c \right) \cdot N_j + \frac{\phi_j^c}{v_j} \cdot \sum_{k=1}^{nc} v_k \cdot N_k \right)$
Matrix form of the diffusion fluxes for two components	$(N) = -[q^{sat}][Đ][\Gamma]^{-1}(\nabla \theta)$ $[q^{sat}] = \begin{bmatrix} q_1^{sat} & 0 \\ 0 & q_2^{sat} \end{bmatrix}$ $[Đ] = \begin{bmatrix} Đ_{1,nc+1} & 0 \\ 0 & Đ_{2,nc+1} \end{bmatrix}$ $[\Gamma]^{-1} = \frac{1}{1-\theta_t} \begin{bmatrix} 1-\theta_2 & \theta_1 \\ \theta_2 & 1-\theta_1 \end{bmatrix}$	$(N_j) = -[D][\Gamma]^{-1}(\nabla \phi_j^*)$ $[D] = \begin{bmatrix} D_{1,NC+1} & 0 \\ 0 & D_{2,NC+1} \end{bmatrix}$ $[\Gamma]^{-1} = \frac{1}{\left(1 + b_1 \cdot \frac{\phi_1^*}{v_1} + b_2 \cdot \frac{\phi_2^*}{v_2}\right) \cdot (1 - \phi_T^c)} \begin{bmatrix} 1-\phi_1^c & -\phi_1^c \cdot \frac{v_2}{v_1} \\ -\phi_2^c \cdot \frac{v_1}{v_2} & 1-\phi_2^c \end{bmatrix} \begin{bmatrix} \frac{q_1^{sat} \cdot b_1}{v_1} & 0 \\ 0 & \frac{q_2^{sat} \cdot b_2}{v_2} \end{bmatrix}$

For equimolar diffusional fluxes, the following constraint must apply:

$$\sum_{j=1}^{nc} N_j = 0 \tag{30}$$

For example, in a two component mixture, inserting Eq. 30 into Eq. 29 entails:

$$\mathcal{D}_{1,nc+1} = \mathcal{D}_{2,nc+1} \tag{31}$$

Equation 31 shows that introducing the Gibbs–Duhem constraint induces a dependence between the Maxwell–Stefan diffusion coefficients. This of course remains true for more than two components. As an example of consequence, binary equimolar diffusion cannot occur for species with different Maxwell–Stefan diffusion coefficients. This is particularly critical for modeling the diffusion behavior when the adsorbent is at, or near saturation, as it is the case for liquid phase adsorption. In that case, equilibrium constraints impose an equimolar diffusion for a binary system (molecule A cannot enter the network as long as molecule B has not left). The model will only be able to represent this phenomenon if $\mathcal{D}_{1,nc+1} = \mathcal{D}_{2,nc+1}$.

It is interesting to note that the saturation hypothesis is not necessary to derive Eqs. 26–31. The interdependence between the diffusion coefficients is formally the same whether the adsorbent is saturated or not. However, Krishna's and our formalism yield the same numerical results when the adsorbent is far from saturation, because in that case the constraints induced by neglecting the solid flux term become negligible. Moreover, assuming that the solid flux is zero yields a dependence between the diagonal diffusion coefficients, whether or not the crossdiffusion coefficients are neglected. This can be easily shown by deriving Eqs. 26–31 without neglecting the crossdiffusion coefficients. Equation 29 becomes:

$$\sum_{j=1}^{nc} \left(\frac{N_j}{\mathcal{D}_{j,nc+1}} + \sum_{\substack{k=1 \\ k \neq j}}^{nc} \frac{\left(\theta_k \cdot N_j - \theta_j \cdot N_k\right)}{\mathcal{D}_{k,j}} \right) = 0 \tag{32}$$

For a binary mixture:

$$\frac{N_1}{\mathcal{D}_{1,nc+1}} + \frac{N_2}{\mathcal{D}_{2,nc+1}} + \left(\frac{1}{\mathcal{D}_{2,1}} - \frac{1}{\mathcal{D}_{1,2}} \right) \cdot \left(\theta_2 \cdot N_1 - \theta_1 \cdot N_2\right) = 0 \tag{33}$$

Since $\mathcal{D}_{2,1} = \mathcal{D}_{1,2}$, interdependence of the diffusion coefficients is confirmed.

The same problem arises with the diffusion model developed by Habgood, which is in fact a simplified version of Krishna's model, where counterdiffusion is not taken into account. The expression of the diffusive flux for binary diffusion as obtained by Habgood[12] is:

$$N_1 = -\frac{RTL_1}{1 - \theta_1 - \theta_2} \cdot \left((1 - \theta_2) \cdot \nabla q_1 + \theta_1 \cdot \nabla q_2 \right) \tag{34}$$

where L_1 is a "proportionality constant," according to the author.

Equation 34 is strictly equivalent to Krishna's formulation (see Table 1), when the Maxwell–Stefan diffusion coefficient is defined by:

$$\mathcal{D}_{1,nc+1} = RTL_1 \tag{35}$$

By contrast, if Eq. 28 (the Gibbs–Duhem equation) is applied to this work's diffusion equation, we get:

$$\phi^c_{nc+1} \nabla \left(\frac{\mu_{nc+1}}{v_{nc+1}} \right) = -\sum_{j=1}^{nc} \left(\frac{1}{D_{j,nc+1}} \left(\phi^c_{nc+1} \cdot N_j - \frac{\phi^c_j}{v_j} \cdot v_{nc+1} N_{nc+1} \right) \right) \tag{36}$$

Introducing Eqs. 22 (flux constraint) and 23 (volume constraint) into the above equation gives (for two adsorbable components):

$$\phi^c_{nc+1} \nabla \left(\frac{\mu_{nc+1}}{v_{nc+1}} \right) = -\frac{1}{D_{1,nc+1}} \cdot \left(N_1 \cdot \left(1 - \phi^c_2\right) + N_2 \cdot \phi^c_1 \cdot \frac{v_2}{v_1} \right) - \frac{1}{D_{2,nc+1}} \cdot \left(N_2 \cdot \left(1 - \phi^c_1\right) + N_1 \cdot \phi^c_2 \cdot \frac{v_1}{v_2} \right) \tag{37}$$

Equation 37 shows that introducing the Gibbs–Duhem constraint in this work's diffusion equation has no consequence on the independence of the diffusion coefficients.

One may wonder about the meaning of the quantities related to the solid nc + 1 in this approach.

Although the quantities v_{nc+1}, N_{nc+1}, and μ_{nc+1} are not operationally defined as separate variables in the present model because they are molar quantities for the solid, their combinations μ_{nc+1}/v_{nc+1} and v_{nc+1}. N_{nc+1} make sense. μ_{nc+1}/v_{nc+1} has the same dimension (J m^{-3}) as the terms q_j μ_j in the Gibbs–Duhem equation and is a sort of volumetric chemical potential of the solid, with some finite value. In the present text, its only use is for the demonstration associated to Eq. 37, and we do not have to calculate it or affect a value to it. v_{nc+1}. N_{nc+1} on the other hand is a volume flux, and has been discussed above. In terms of physical interpretation, the right-hand side of Eq. 37 represents the force exerted by the two species on the solid. For the Gibbs–Duhem constraint to be respected, the friction force exerted by any diffusing species on the solid has to be compensated by a reciprocal force. In our model, this force is related to a flux of the solid and logically associated to a gradient of some chemical potential. It should be emphasized again that this solid flux is relative to the barycentre of the volume of all species (thus including the solid), which constitutes the reference frame for the definition of the fluxes in our model (of course, there would be no solid flux if the solid itself was taken as reference). This question of reference frame is often the source of confusion in the formulation of coupled diffusion in a dusty gas approach.

Finally, we keep in mind that these variables appear in intermediate equations—but are eliminated in the final equations such as the flux Eq. 24 by taking into account the global mass balance.

Single Component Diffusion. For a single component, the diffusion Eq. 24 reduces to:

$$N_1 = -\left(\frac{q_1^{\text{sat}} b_1}{1 + b_1 \frac{\phi_1^*}{v_1}}\right) D_{1,\text{nc}+1} \left(\frac{\partial \phi_1^*}{\partial r_c}\right) \tag{38}$$

Changing the state variables (ϕ_1^* to q_1) in Eq. 38 yields the well-known Darken relation[7]:

$$N_1 = -\left(\frac{D_{1,\text{nc}+1}}{1 - \theta_1}\right) \left(\frac{\partial q_1}{\partial r_c}\right) \tag{39}$$

For one component, and for this case only, the two formulations (Krishna's and this work's) are equivalent.

Estimability of Parameters. For a system at (or near) saturation, the Langmuir Eq. 14 can be reduced by considering that $\sum_{j=1}^{\text{nc}} b_j C_j >> 1$, which gives:

$$\phi_j^{c,k} = \frac{q_j^{\text{sat}}.b_j.\phi_j^{*,k}}{\sum_{l=1}^{\text{nc}} \frac{b_l \phi_l^{*,k}}{v_l}} \quad j = 1, \ldots, \text{nc} \tag{40}$$

This equation can be rewritten as follows:

$$\phi_j^{c,k} = \frac{q_j^{\text{sat}}.\phi_j^{*,k}}{\frac{\phi_j^{*,k}}{v_j} + \sum_{\substack{l=1 \\ l \neq j}}^{\text{nc}} \frac{b_l \phi_l^{*,k}}{b_j \; v_l}} \quad j = 1, \ldots, \text{nc} \tag{41}$$

On the basis of this equation, an estimability study carried out at the microporous phase level shows that, at saturation and for a mixture of nc species, there are only (nc − 1) independent estimable parameters:

- The ratio of the Langmuir coefficients b_j/b_1, j = 2,nc.
- The Maxwell–Stefan diffusion coefficients $D_{j,\text{nc}+1}$, j = 1,nc.

Only coadsorption isotherms can be estimated from liquid phase breakthrough curves. Therefore, in the experimental part that follows, only the Langmuir coefficients ratios (relative to 2-methylpentane) will be evaluated.

Numerical solution of model equations

The set of partial differential equations is first reduced to a set of ordinary differential equations by applying an orthogonal collocation technique to the spatial coordinate corresponding to the crystal radius, using the subroutines JCOBI and DFOPR developed by Villadsen and Michelsen.[13] Axial dispersion along the bed length is represented by the series of CSTR. The resulting ordinary differential algebraic system of equations is solved using the DDASPG integration subroutine (IMSL library), based on the Petzold-Gear BDF method. Matrix 15 is inverted by the DLINRG inversion subroutine (IMSL library).

Experimental Methods

All the parameters relative to the physical characteristics of the adsorbent, the geometry of the columns and the external mass transfer parameters have been determined independently and can be found in Table 3.

Adsorbent characterization

The silicalite crystals used in this study were supplied by Zeolyst International. The Si/Al ratio, measured by X-ray fluorescence, is 500 ± 50% (experimental uncertainties are important for such a high ratio). The few H^+ cations initially present in the zeolite framework were replaced by Na^+ cations using the conventional ion exchange technique and subsequent washing. Scanning electron microscopy showed that the crystals are spheroïdal with a mean crystal radius of $R_c = 0.75\ 10^{-6}$ m.

This zeolite was pelletized with a silica binder in the Institut Français du Pétrole, then cut and sieved. Resulting pellets are small cylinders with a diameter of 0.85 mm and a mean length of 0.8 mm. For model simplification, particles were supposed to be spherical with a mean radius of $R_p = 0.41 \times 10^{-3}$ m. The binder ratio, determined from *n*-hexane adsorption gravimetric uptake experiments performed with both crystals and pellets, is 20%. In the rest of this article, the value of all the thermodynamic parameters is always corrected of the binder ratio. The porosity of the particles was measured by mercury porosimetry ($\varepsilon_p = 0.34$).

Prior to experiments, the sample is activated in a nitrogen stream for 3 h at 300°C.

Experimental setup

Breakthrough experiments, which allow to evaluate both thermodynamic and mass transfer data, were carried out according to standard procedures as described in literature.[3] The dynamic adsorption unit is described in Figure 1. A stainless steel column (L = 1 m and $S = 0.848 \times 10^{-4}$ m^2) is packed with a known mass of pellets and placed into the oven. The interstitial porosity is calculated from the mass and the density of the pellets, giving $\varepsilon_i = 0.29$. First, the column is filled with the so-called solvent (or desorbent), which is also an adsorbable species. Then, the feed is injected into the column, until complete breakthrough (outlet concentration = inlet concentration). During the experiment, the whole column is maintained at 35 bar and 185°C. Liquid fractions of the effluent are collected and analyzed by a gas chromatograph with a FID detector and a PONA analytical column. The concentrations at the outlet of the column are plotted as fractional volumes as a function of time; they are called "breakthrough curves." Reverse breakthrough experiments consist in injecting the solvent into a column filled with the feed.

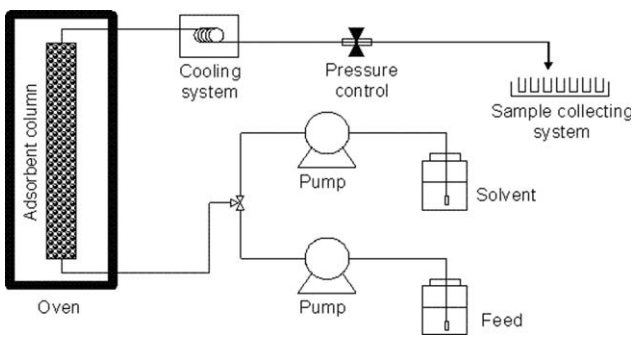

Figure 1. Experimental setup.

Table 2. Experimental Conditions for the Different Runs

Run	Feed (mass %)	Desorbent	Flow rate (cc/min)
	3MP/2MP	2MP	10
1	100/0		
2	70/30		
3	30/70		
	3MP/2MP	2MP	3
4	100/0		
5	70/30		
6	30/70		
	3MP/23DMB	2MP	10
7	0/100		
8	25/75		
9	50/50		
10	75/25		
	3MP/22DMB	2MP	10
11	0/100		
12	15/85		
13	30/70		
14	50/50		
	3MP/22DMB	2MP	5
15	15/85		

The adsorbates are 2-methylpentane (2MP) and 3-methylpentane (3MP) purchased from Fluka Chemika, 2,3-dimethylbutane (23DMB) and 2,2-dimethylbutane (22DMB) purchased from SAFC. The specified purities are over 99%. All these adsorbates were used without further purification.

Macroporous mass transfer coefficients

The lumped macroporous mass transfer coefficient k^m was calculated using Eq. 7 (the fluid film around the pellet is neglected):

$$k^{\mathrm{m}} = \frac{5.\varepsilon_p.D^{\mathrm{mac}}}{R_p} \tag{42}$$

with

$$D^{\mathrm{mac}} = \frac{D_m}{\tau} \tag{43}$$

where D_m is the molecular diffusion coefficient, considered the same for all components since the molecules are very similar ($D_m = 0.2 \times 10^{-8}$ m^2/s) and τ is the tortuosity factor, fixed at a value of 3.8.

This finally gives $k_m = 2.4 \times 10^{-5}$ m/s.

Table 3. Model Input Parameters

R_c (m)	0.75×10^{-6}
R_p (m)	0.41×10^{-3}
ε_i	0.29
ε_p	0.34
τ_{binder}	20%
L_{bed} (m)	1.0
S_{bed} (m^2)	8.48×10^{-5}
N_{CSTR}	150
k^{m} (m s^{-1})	2.4×10^{-5}
$v_{3\mathrm{MP}}$ (m^3 mol^{-1})	1.86×10^{-4}
$v_{2\mathrm{MP}}$ (m^3 mol^{-1})	1.93×10^{-4}
$v_{23\mathrm{DMB}}$ (m^3 mol^{-1})	1.87×10^{-4}

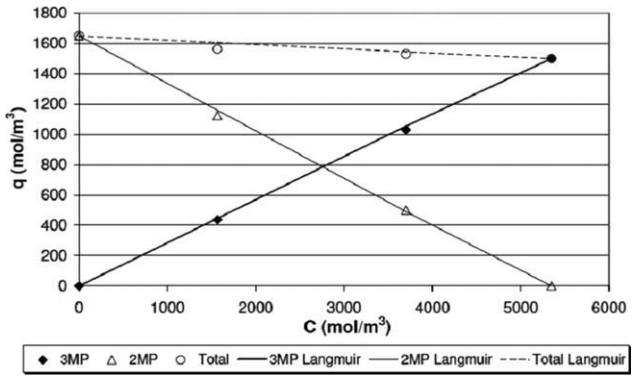

Figure 2. 2MP/3MP coadsorption isotherm.

Results and Discussion

A complete set of breakthrough curves were measured using the above described experimental setup. A summary of all the runs with the corresponding experimental conditions can be found in Table 2. Some of the experiments were used for parameter estimation and the others for model validation. As previously explained, only the ratios of Langmuir isotherm parameters and the "diagonal" Maxwell–Stefan diffusion coefficients were estimated from the breakthrough curves. The other parameters, listed in Table 3, have been determined independently.

Langmuir parameters estimation

The 3MP/2MP and 3MP/23DMB coadsorption isotherms were determined by making global mass balances on breakthrough curves with different feed compositions, using the well-known first moment method. For 3MP/2MP, Experiments 1–3 were used, for 3MP/23DMB, Experiments 7–10. The resulting coisotherms can be found in Figure 2 (3MP/2MP) and Figure 3 (3MP/23DMB). The isotherms were fitted using the Langmuir isotherm, with the hypothesis that $b_i \cdot C_i \gg 1$ (Eq. 41), and the fitted Langmuir parameters are listed in Table 4. As can be seen in Figures 2 and 3, the simplified Langmuir model represents very well the experimental results, which confirms that the adsorbent is very close to saturation.

The 2MP/3MP coadsorption isotherm is linear with $\frac{b_{3\mathrm{MP}}}{b_{2\mathrm{MP}}} = 1$, because the interactions of the two isomers with the

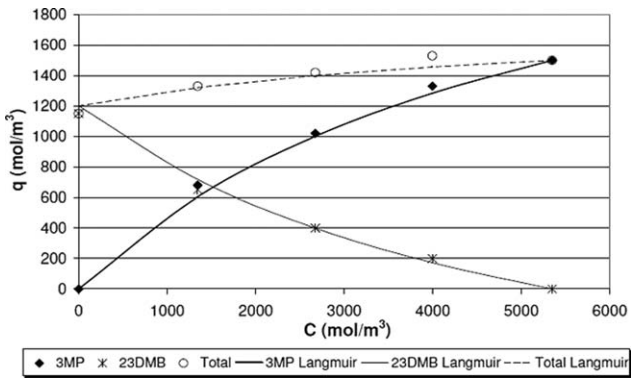

Figure 3. 3MP/23DMB coadsorption isotherm.

Table 4. Estimated Langmuir Parameters and Diffusivities for Each Species

	3MP	2MP	23DMB
q_j^{sat} (mol m^3)	1500	1650	1200
q_j^{sat} (molecule per unit cell)	4.8	5.3	3.8
b_j/b_{2MP}	1.0	–	0.55
$D_{j,nc+1}$ (m^2 s^{-1})	3.6×10^{-15}	2.1×10^{-15}	6.1×10^{-16}

silicalite structure is very comparable. On the contrary, the 3MP/23DMB isotherm is nonlinear and favorable to 3MP with $\frac{b_{23DMB}}{b_{3MP}} = 0.55$: the dibranched isomer suffers from severe steric hindrance in the silicalite porosity, therefore cannot develop very strong interactions with the solid. The Langmuir coefficients ratios obtained in this study can be compared with the results of Cavalcante and Ruthven,[14] who obtained, for temperatures comprised between 150 and 200°C: $0.74 < \frac{b_{3MP}}{b_{2MP}} < 0.89$ and $0.2 < \frac{b_{23DMB}}{b_{3MP}} < 0.25$. The tendencies are the same for the two studies, even though the thermodynamic selectivities determined by Cavalcante and Ruthven are higher. This can be explained by the different experimental conditions (gas phase experiments at low loadings vs. liquid phase experiments, pure component experiments vs. mixtures).

The pure component saturation capacities are in the order 2MP > 3MP > 23DMB, which is also in agreement with the data of Cavalcante and Ruthven.[14] The saturation capacities values obtained in the literature by extrapolation from low loading data are always smaller than our results: for temperatures between 150 and 200°C, Cavalcante and Ruthven,[14] Jolimaitre et al.,[15] and Lemaire et al.[16] all obtain q^{sat} values between 3 and 3.7 molecules per cell for 2MP and 3MP and between 1.4 and 3.4 molecules per cell for 23DMB. However, molecular simulations[17] at 190°C and 35 bar yield a 3MP adsorption capacity of 4.7 molecules per cell, much closer to our experimental value of 4.8 (Table 4). To our knowledge, no CBMC simulations are available for 23DMB. However, our fitted value of 3.8 molecules per cell is coherent with the theoretical value of 4 molecules per cell, corresponding to the channel intersection sites.

The 22DMB Langmuir parameters could not be estimated from our experimental results, because the number of 22DMB molecules that penetrate into the adsorbent during the breakthrough curve duration is nearly negligible. Typically, for Runs 11–15, the adsorbed quantities derived from the first moment analysis are always smaller than 0.5 molecules per cell, which is very close to our experimental error. This demonstrates that for very slow diffusing species, breakthrough curves are not the appropriate experimental setup to measure diffusion coefficients.

Diffusion coefficients estimation

Once the Langmuir thermodynamic parameters are fixed, the diffusion coefficients are the only unknown parameters of the model. The 3MP, 2MP, and 23DMB diffusion coefficients can then be estimated using the least-square fit method. Only binary breakthrough curves were used for this fitting (Run 1 for 2MP and 3MP and Run 7 for 23DMB). The results can be found in Table 4. Comparison between

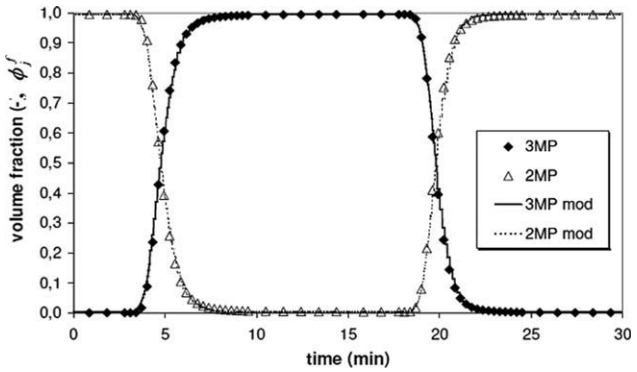

Figure 4. 3MP/2MP breakthrough and reverse breakthrough curves (Run 1).

the experiments and the model using the fitted parameters are shown in Figures 4 and 5. As can be seen from these figures, the model well represents the experimental results, particularly for the 2MP/3MP breakthrough curve (Figure 4). For 23DMB, the fit is not as accurate as for the monobranched molecules. This point will be discussed more thoroughly in the next section of this article.

The diffusion coefficients are in the order $D_{3MP} > D_{2MP} > D_{D23DMB}$. As expected, the monobranched isomers diffuse faster than the dibranched one. However, our results suggest that 3MP diffuses faster than 2MP, which is not in agreement with some other literature studies.[18,19] Since the diffusion coefficients of the two molecules are very close, a slight experimental error may result in an apparent inversion of the diffusion orders. Koriabkina[20] found that diffusion of 2MP becomes smaller than that of 3MP for $T > 180$°C. Since this work was carried out at 185°C, this might be another explanation.

It is difficult to compare our diffusion coefficients with literature results, since on one hand literature values are very dispersed and on the other hand the models used to describe the diffusion process are different. Thus, we believe that only the comparison of orders of magnitude and of the values relative to one another make sense. This well known but not entirely resolved problem of comparison of diffusion coefficients obtained by different methods has been extensively discussed by Kärger and Ruthven.[21] Still, the 3MP and 2MP diffusivity values given here are close to that

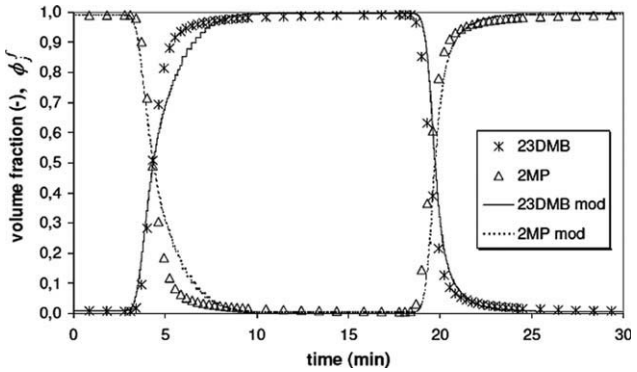

Figure 5. 23DMB/2MP breakthrough and reverse breakthrough curves (Run 7).

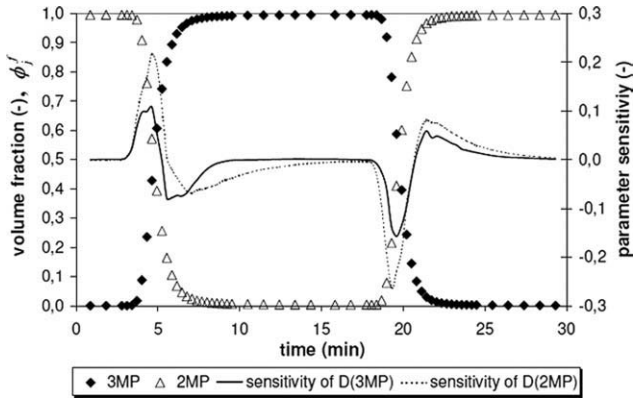

Figure 6. 2MP and 3MP diffusion coefficients sensitivities (Run 1).

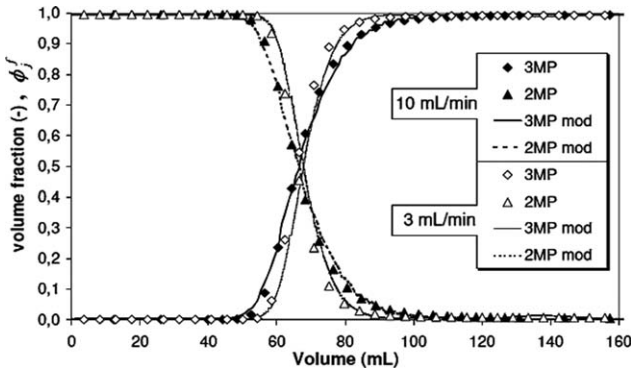

Figure 8. Effect of flow-rate: experimental and simulated 3MP/2MP breakthrough curves (Runs 1 and 4).

obtained by Jolimaitre et al.[15] and Lemaire et al.[16] for the same silicalite sample (even though the experimental conditions and the models hypothesis are quite different).

In a previous article,[22] we presented results for the same system. The estimated diffusion coefficients for 2MP and 3MP were slightly different ($D_{2MP} = D_{3MP} = 1 \times 10^{-14}$ m^2/s), because our model was at that time less elaborate: the adsorbed phase saturation q^{sat} and the molar volumes were the same for all species, the number of CSTR was not optimal, mass transfer in the macropores was represented by a simpler LDF model, the variation of the fluid velocity was not taken into account. This emphasizes the necessity to represent precisely all the mass transfer resistances in the system to estimate microporous diffusion coefficients from breakthrough curves.

A parameter sensitivity study has been carried out, by calculating the influence of a variation of the estimated parameters on the model output. A parameter P is experimentally identifiable if (1) its sensitivity is not negligible $\frac{\partial M(t)}{\partial P_i} \neq 0$ and (2) its sensitivity is not proportional to the sensitivity of any other parameter $\frac{\partial M(t)}{\partial P_i} \neq A \cdot \frac{\partial M(t)}{\partial P_k} \quad \forall k \neq i$, where $M(t)$ is the output of the model, P_i the input parameters and A a constant (independent of time). The results are shown in Figures 6 and 7. In these figures, the sensitivity is calculated using the formula $\frac{M(t)|_{Pi} - M(t)|_{Pi+\Delta Pi}}{M(t)|_{Pi}}$ and has therefore no dimension. The diffusion coefficients of the three species are clearly sensitive in our experimental conditions. Moreover, the 2MP and 3MP sensitivities are distinct: the 2MP diffusion coefficient is more sensitive at the end of the breakthrough curve. All the diffusion coefficients are therefore estimable in our experimental conditions.

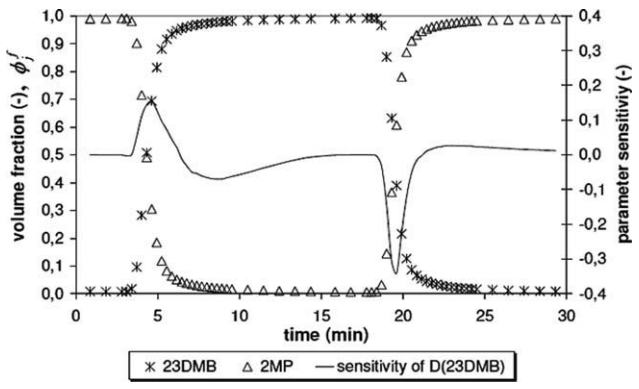

Figure 7. 23DMB diffusion coefficient sensitivity (Run 7).

Simulation results and discussion

The experiments listed in Table 2 (except Runs 1 and 7, which were used in the fitting procedure) have been simulated using the previously estimated parameters, i.e., with no further fitting.

The influence of the feed flow rate on the 2MP/3MP breakthrough curves is depicted in Figure 8. It appears that the simulations are in very good agreement with the experimental results in the range of flow-rate considered. Figure 9 illustrates the effect of changes of feed composition on both experimental and simulated breakthrough curves for different 2MP/3MP binary mixtures. Once again, agreement between experiments and simulations is very satisfactory. Our model represents well the 2MP/3MP system over a wide range of experimental conditions.

Figure 10 on the other hand shows parts of ternary experiments in which the binary mixture 3MP + 23DMB is displaced or displaces 2MP. For clarity, only the 23DMB concentrations are shown. It can be seen that there is a slight

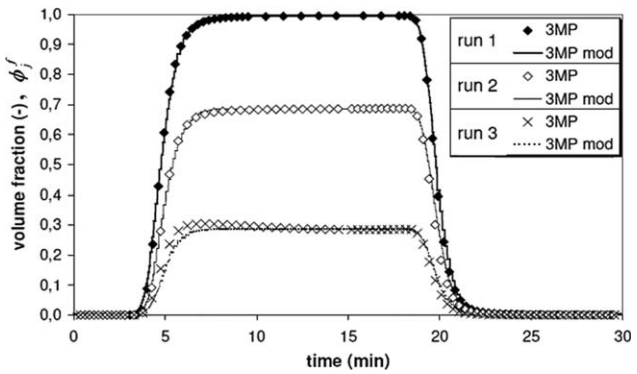

Figure 9. Effect of feed composition: experimental and simulated 3MP/2MP breakthrough and reverse breakthrough curves (only 3MP is shown on this graph).

difference between simulated and experimental breakthrough curves. This discrepancy increases with 23DMB concentration in the feed. Moreover, the shapes of the ternary breakthrough curves involving 23DMB seem to indicate an inversion of the apparent selectivity. This phenomenon is more visible when the breakthrough curves are normalized and compared with the reverse breakthrough curves. An example of such a curve, corresponding to Run 8, is depicted in Figure 11 (please note that on this figure, the reverse breakthrough curve is inverted to facilitate its comparison with the breakthrough curve). For 23DMB and 2MP, the breakthrough and inverse breakthrough curves can be perfectly superimposed, which is a characteristic of linear exchange isotherms. On the contrary, the 3MP breakthrough front is dispersive whereas its reverse breakthrough front is compressive. It seems that the exchange between 3MP and 2MP, which is linear in the binary system, becomes unfavorable to 3MP in presence of 23DMB. To explain this phenomenon, which cannot be predicted from the 2MP/3MP and 2MP/23DMB exchange isotherms, the following hypothesis can be proposed:

- An inversion of the thermodynamic selectivity. In this case, our Langmuir thermodynamic model is not adapted.
- A complex diffusion behavior, not taken into account by our model. For that kind of mixtures, the Maxwell–Stefan binary exchange diffusion coefficients D_{ij}—which represent the interactions between components i and j—might not be negligible anymore.

This problem is a very good illustration of the difficulties encountered when dealing with multicomponent diffusion in zeolites, especially in the presence of slow-diffusing species. Thermodynamics and kinetic phenomenon are coupled in such an intricate manner that it is sometimes difficult to determine the real limitations of the models.

Conclusion

This work proposes a model for coupled adsorption when thermodynamic, steric, and diffusional interactions occur simultaneously. This model, an evolution of Krishna's Maxwell–Stefan approaches, is appropriate in cases where the adsorbent is at or near saturation (adsorption from the liquid phase, all species adsorbable) and avoids contradictions or difficulties met when earlier models are extrapolated to this situation. It also accounts for different saturation capacities and different intrinsic diffusivities. We believe this model to be fully consistent, both from the thermodynamic and the diffusion points of view. Let us discuss this point in detail.

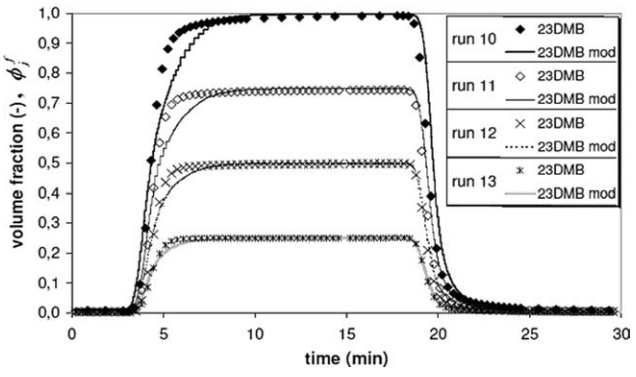

Figure 10. Effect of feed composition: experimental and simulated (3MP + 23DMB)/2MP breakthrough and reverse breakthrough curves (only 23DMB is shown on this graph).

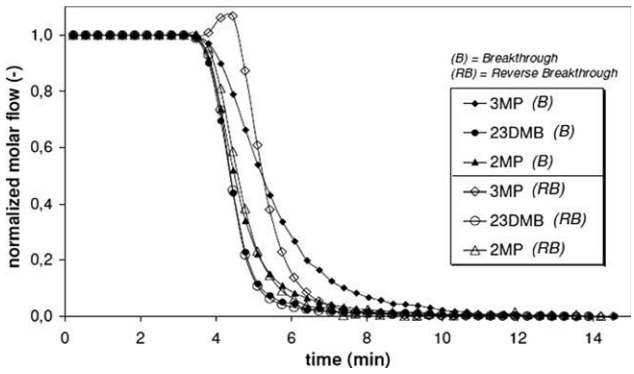

Figure 11. Normalized experimental breakthrough and inverted reverse breakthrough curves for Run 8.

It is usually admitted that multicomponent Langmuir equilibria with unequal saturation capacities are thermodynamically inconsistent, i.e., are incompatible with the Gibbs–Duhem constraint. However, the particular definition of the concentration variables and the detailed accounting of the volume constraints implemented here allow a Langmuir-type equilibrium to be formulated with different saturation capacities for the components, while the Gibbs–Duhem constraint is still satisfied.

In the general Maxwell–Stefan diffusion framework, there are nondiagonal crossdiffusion coefficients D_{ij}. Using the hypothesis that diffusion takes place with no mutual interaction between the species is physically sound in the present case, because the size of the molecules is very close to that of the microporosity. Only nc "diagonal" diffusion coefficients, expressing the interaction of each component with the solid matrix, are necessary, i.e., there are no crossdiffusional coefficients. This of course greatly reduces the number of diffusion coefficients to be determined from experiments, and only in this framework is it reasonable to use breakthrough experiments for that purpose. On the other hand, one has to be careful that the remaining nc coefficients are independent, in spite of the different constraints, in particular of Gibbs–Duhem applying to the gradients of chemical potentials. This is achieved here by a proper formulation of the dusty gas model, where the flux of the solid "species" is not cancelled, as was done in earlier literature. This is possible and makes sense because of the use of volume variables and of the inclusion of the solid matrix volume in the reference frame for the diffusion fluxes.

It is important to note that the fact of having a diagonal matrix of diffusion coefficients does not mean that the diffusion of the different species is decoupled. The coupling is brought by the volume constraints and by the equilibrium. The diffusional transfer process must be considered as a global phenomenon where the thermodynamic and steric constraints cannot be dissociated, but instead interact to

shape the nondiagonal matrix relating the fluxes and the driving forces, However, the nc diffusion coefficients of the model are independent, each representing in principle the interaction of the species at hand with the solid matrix. This independence property is a necessary (but not sufficient!) condition for these coefficients to be determinable by independent single component experiments, a challenge still to be satisfied.

Breakthrough experiments were carried out with the purpose to test the model both for parameter estimation and for experimental representation and prediction. Breakthrough curves for mixtures of 2-methylpentane (2MP), 3-methylpentane (3MP), 2,3-dimethlybutane (23DMB), and 2,2-dimethylbutane (22DMB) in the liquid phase have been measured at 185°C.

By making mass balances on the breakthrough curves, the 2MP/3MP and 3MP/23DMB coadsorption isotherms have been determined. Using the new model, diffusivities of 2MP, 3MP, and 23DMB have been estimated from binary component breakthrough curves. The parameters were validated by simulating a whole set of breakthrough curves in different experimental conditions.

All the experiments can be well simulated with our set of parameters, except when the feed is concentrated in 23DMB. In that case, an apparent inversion of selectivity between 23DMB and 3MP occurs for which the present model seems to fail.

For 22DMB, it was not possible to carry out a valid parameter estimation, because the quantity of 22DMB adsorbed during the breakthrough curves is nearly negligible. Most probably, the diffusion coefficient of that species is too small, so that the molecules do not have the time to penetrate into the micropores.

The particular system investigated (mono- and di-branched hydrocarbons in silicalite) at the same time validates the approach proposed and illustrates its thermodynamic and kinetic limits. On the thermodynamic side, when and if selectivity reversals occur, the Langmuir isotherm probably has to be abandoned, with the consequence of introducing more equilibrium parameters. On the diffusional side, in the presence of species with very small diffusivity (here, 22DMB), the diffusion parameters may be impossible to estimate from the same breakthrough experiments. An alternative method, based on cyclic inverse chromatography, will be proposed in an oncoming article.

Notation

b_j = thermodynamic Langmuir coefficient of component j (m^3 mol^{-1})
C_j^* = concentration of component j in the hypothetic fluid at equilibrium with the adsorbed phase (mol m^{-3})
C_T = total concentration in the fluid phase (mol m^{-3})
C_T^* = total concentration in the hypothetic fluid at equilibrium with the adsorbed phase (mol m^{-3})
$D_{j,nc+1}$ = this work's Maxwell–Stefan diffusion coefficient for component j (m^2 s^{-1})
$\mathcal{D}_{j,nc+1}$ = Krishna's Maxwell–Stefan diffusion coefficient for component j (m^2 s^{-1})
D_{ij} = Maxwell–Stefan binary exchange diffusion coefficient (m^2 s^{-1})
k_j^c = mass transfer coefficient of component j at the surface of the crystals (m s^{-1})
k_j^f = mass transfer coefficient of component j at the surface to the pellets (m s^{-1})
k_j^m = lumped mass transfer coefficient of component j at the surface of the pellet as defined by Eq. 7 (m s^{-1})
L = packed column length equivalent to one CSTR $\left(L = \frac{L_{bed}}{N_{CSTR}}\right)$ (m)
L_{bed} = packed column length (m)
nc = number of components
N_j^c = molar flux of component j in the crystals (mol m^{-2} s^{-1})
N_j^{mic} = molar flux of component j at the surface of the crystals (mol m^{-2} s^{-1})
N_T^{mac} = total molar flux at the surface of the pellets (mol m^{-2} s^{-1})
N_j^{mac} = molar flux of component j at the surface of the pellets (mol m^{-2} s^{-1})
N_{CSTR} or NZ = number of continuous stirred tank reactors (CSTRs)
q_j^{sat} = adsorbed phase concentration of component j at saturation (mol m^{-3} of solid)
q_j = molar concentration of species j in adsorbed phase (mol m^{-3} of solid)
r_c = crystal radius coordinate (m)
R_c = crystal radius (m)
R_p = pellet radius (m)
S = section of the column (m^2)
T = temperature (K)
x_j = molar fraction of species j
v_j = molar volume of species j (m^3 mol^{-1})
u_t^0 = superficial velocity of the fluid at the bed inlet (m s^{-1})
u_t^k = superficial velocity of the fluid in the kth CSTR (m s^{-1})
α^k = nondimensional superficial fluid velocity in the kth CSTR as defined by Eq. 2
ε_i = extragranular porosity
ε_p = intragranular macroporosity
ϕ_j^c = adsorbed phase volume fraction of component j
$\bar{\phi}_j^c$ = average adsorbed phase volume fraction of component j in the crystal
$\phi_j^{f,0}$ = volume fraction of component j in the feed
ϕ_j^* = nondimensional concentration of component j in the hypothetic fluid at equilibrium with the adsorbed phase as defined by Eq. 13
ϕ_j^m = volume fraction of component j in the macroporosity
ϕ_j^f = volume fraction of component j in the extragranular fluid phase
θ_j = fractional occupancy of component j in the adsorbed phase
θ_t = total fractional occupancy in the adsorbed phase
μ_j^c = chemical potential of species j in the adsorbed phase (J mol^{-1})
μ_j^* = chemical potential of species j in the hypothetic fluid at equilibrium with the adsorbed phase (J mol^{-1})

Literature Cited

1. Krishna R. Multicomponent surface diffusion of absorbed species: a description based on the generalized Maxwell-Stefan equations. *Chem Eng Sci*. 1990;45:7:1779–1791.
2. Taylor R, Krishna R. *Multicomponent Mass Transfer*. New York: Wiley, 1993.
3. Ruthven DM. *Principles of Adsorption and Adsorption Processes*. New York: Wiley, 1984.
4. Tayakout-Fayolle M, Jolimaitre E, Jallut C. Consequence of structural identifiability properties on state-model formulation for linear inverse chromatography. *Chem Eng Sci*. 2000;55:2945–2956.
5. Leinekugel-le-Cocq D, Tayakout-Fayolle M, Le Gorrec Y, Jallut C. A double linear driving force approximation for non-isothermal mass transfer modeling through bi-disperse adsorbents. *Chem Eng Sci*. 2007;62:4040–4053.
6. Krishna R, Wesselingh JA. The Maxwell-Stefan approach to mass transfer. *Chem Eng Sci*. 1997;52:861–911.
7. Chen YD, Yang RT. Concentration dependence of surface diffusion and zeolitic diffusion. *AIChE J*. 1991;37:1579–1582.

8. Krishna R. Exploiting configurational entropy effects for separation of hexane isomers using silicalite-1. *Trans I ChemE*. 2001;79:182–194.
9. Krishna R, Baur R. Modelling issues in zeolite based separation processes. *Sep Purif Technol*. 2003;33:213–254.
10. Krishna R. A united approach to the modelling of intraparticule diffusion in adsorption processes. *Gas Sep Purif*. 1993;7:91–104.
11. Krishna R, van Baten JM. Diffusion of alkane mixtures in zeolites: validating the Maxwell-Stefan formulation using MD simulations. *J Phys Chem B*. 2005;109:6386–6396.
12. Habgood HW, Round GF, Newton R. A numerical analysis of surface diffusion in a binary adsorbed film. *Sep Sci*. 1966;1:219–244.
13. Villadsen J, Michelsen ML. *Solution of Differential Equation Models by Polynomial Approximation*. NJ: Prentice-Hall, Englewood Cliffs, 1978.
14. Cavalcante CL Jr, Ruthven DM. Adsorption of branched and cyclic paraffins in silicalite. I. Equilibrium. *Ind Eng Chem Res*. 1995;34:177–184.
15. Jolimaitre E, Tayakout-Fayolle M, Jallut C, Ragil K. Determination of mass transfer and thermodynamic properties of branched paraffins in silicalite by inverse chromatography technique. *Ind Eng Chem Res*. 2001;40:914–926.
16. Lemaire E, Decrette A, Bellat JP, Simon JM, Méthivier A, Jolimaître E. Adsorption and diffusion of linear and dibranched C6 paraffins in a ZSM-5 zeolite. *Stud Surf Sci Catal*. 2002;142:1571–1578.
17. Shenk M, Vidal SL, Vlugt TJH, Smit B, Krishna R. Separation of alkane isomers by exploiting entropy effects during adsorption in silicalite-1: a configurantional-bias Monte Carlo study. *Langmuir*. 2001;17:1558–1570.
18. Cavalcante CL Jr, Ruthven DM. Adsorption of branched and cyclic paraffins in silicalite 2 kinetics. *Ind Eng Chem Res*. 1995;34:185–191.
19. Zhu W, Kapteijn F, Moulijn JA. Diffusion of linear and branched C6 alkanes in silicalite-1 studied by the tapered element oscillating microbalance. *Microporous Mesoporous Mater*. 2001;47:157–171.
20. Koriabkina AO. Diffusion of Alkanes in MFI-Type Zeolites, PhD Thesis, Technische Universiteit Eindhoven, Eindhoven, The Netherlands, 2003.
21. Kärger J, Ruthven DM. *Diffusion in Zeolites and Other Microporous Solids*. New York: Wiley, 1992.
22. Lettat K, Jolimaitre E, Tayakout M, Méthivier A, Tondeur D. Codiffusion with a slow species in zeolites: cyclic experimentation and advanced modeling. *Adsorption*. 2008;14:475–484.

Manuscript received Nov. 24, 2009, and revision received Mar. 11, 2010.